Modeling of CO_2 Mass Transport Across a Hollow Fiber Membrane Reactor Filled with Immobilized Enzyme

Ya-Tao Zhang
Dept. of Chemical and Biological Engineering, Zhejiang University, Hangzhou 310027, P.R. China

School of Chemical Engineering and Energy, Zhengzhou University, Zhengzhou 450001, P.R. China

Xing-Guo Dai and Guo-Hua Xu
Dept. of Chemical and Biological Engineering, Zhejiang University, Hangzhou 310027, P.R. China

Lin Zhang
Dept. of Chemical and Biological Engineering, Zhejiang University, Hangzhou 310027, P.R. China

Engineering Central of Membrane and Water Treatment, MOE, Hangzhou 310027, P.R. China

Hao-Qin Zhang and Jin-Dun Liu
School of Chemical Engineering and Energy, Zhengzhou University, Zhengzhou 450001, P.R. China

Huan-Lin Chen
Dept. of Chemical and Biological Engineering, Zhejiang University, Hangzhou 310027, P.R. China

Engineering Central of Membrane and Water Treatment, MOE, Hangzhou 310027, P.R. China

DOI 10.1002/aic.12732
Published online August 5, 2011 in Wiley Online Library (wileyonlinelibrary.com).

The enzyme-based contained liquid membrane reactor to capture CO_2 from the closed spaces is a very complicated process with large numbers of interdependent variables. A theoretical and experimental analysis of facilitated transport of CO_2 across a hollow fiber membrane reactor filled with immobilized carbonic anhydrase (CA) by nanocomposite hydrogel was presented. CO_2 concentration profiles in the feed gas phase and the membrane wall were achieved by numeric simulation. The effects of CO_2 concentration, CA concentration, and flow rate of feed gas on CO_2 removal performance were studied in detail, and the model solution agrees with the experimental data with a maximum deviation of up to 18.7%. Moreover, the effect of CO_2 concentration on the required membrane areas for the same CO_2 removal target (1 kg/day) was also investigated. This could provide real-world data and scientific basis for future development toward a final efficient CO_2 removal device. *AIChE J,* 58: 2069–2077, 2012
Keywords: gas purification, mass transfer, mathematical modeling, membrane separations

Introduction

Carbon dioxide (CO_2), a major greenhouse gas, is the major contributor to global warming.[1] Therefore, it is very important to capture and subsequently store CO_2 in a cost-effective and safe approach. On the other hand, control of CO_2 within a certain range is an important task, such as closed life-support systems. Now, CO_2 capture or removal technologies used in the closed spaces are mainly classified into three categories: physical adsorption including molecular sieve and activated carbon,[2] chemical absorption including metal oxides, solid and liquid amines,[3] and biological approaches including microalgae and higher order plants.[4–6] However, these systems have some limitations, such as, possible poisonous substance produced during the regeneration for amines, large quantities of consumption for metal oxides, corresponding large volume and weight due to the predesiccation for molecular sieve, and need to be cultured in water system for microalgae. Importantly, as is well known, CO_2 removal technologies in life-support systems must be safe and reliable.[7] In contrast to the previously described methods, membrane technologies, especially, liquid membranes are attractive in CO_2 capture or separation, typically for low-concentration CO_2 because they decrease transport resistance so that high permeance is achieved together with high selectivity.[8]

However, the reaction must be enhanced by the use of a catalyst that fosters the conversion of CO_2 to bicarbonate to make it practical. Carbonic anhydrase (CA) is known to be the fastest catalyst for the reaction. CA catalyzes the reversible hydration of CO_2 by a two-step process. In the first step, CA hydrolyzes H_2O to capture a hydroxyl releasing a

Correspondence concerning this article should be addressed to L. Zhang at linzhang@zju.edu.cn.

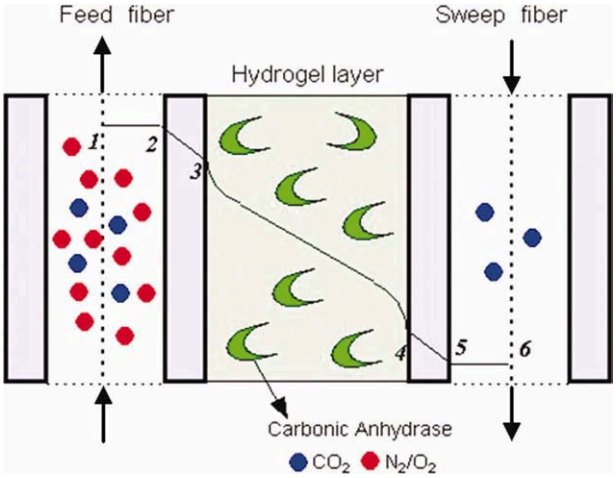

Figure 1. CO_2-facilitated transport process in the hollow fiber membrane reactor filled with immobilized CA enzyme.

[Color figure can be viewed in the online issue, which is available at wileyonlinelibrary.com.]

proton. In the second step, the hydroxyl attacks the carbonyl bond of CO_2 to yield bicarbonate and the unreacted enzyme. The hydration step occurs at the CO_2-rich side. At the CO_2-lean side, the reverse reactions occur, liberating CO_2.[9–11]

Using CA as a catalyst, the design of an immobilized liquid membrane (ILM) or a supported liquid membrane (SLM) has shown the potential to remove low-concentration CO_2. Enns[12] showed that CA, in the presence of a phosphate buffer, could increase CO_2 transfer across a SLM (150-μm thick) by as much as 500-fold depending on pH and CA concentration. Suchdeo and Schultz[13] reported a theoretical and experimental analysis of facilitated transport of CO_2 across a membrane containing $NaHCO_3$ and CA. In the presence of CA (0.1 mg/mL) and 1 M $NaHCO_3$, the CO_2 flux across a 0.02-cm membrane was over threefold higher than the corresponding flux in the absence of enzyme. From experiments at various enzyme concentrations and membrane thickness, it appeared that the apparent CO_2 reaction rate was directly proportional to the enzyme concentration. However, in the subsequent 2 decades, none of these succeeded in reporting a stable, high-efficiency design. One of the important reasons was the instability of SLM or ILM due to evaporative loss and subsequent deactivation of the chemical facilitator.[14] Later, SLM or ILM evolved into contained liquid membranes (CLMs).[15] In CLM operations, a thin film of water or aqueous solution is held in the interstitial space between two independent sets of intimately commingled hydrophobic microporous hollow fibers. One set of fibers carries a feed gas, and the other set carries a sweep gas. The stability of CLM design has been enhanced greatly by holding the aqueous solution within the interstitial space of hydrophobic surfaces. Cowan et al.[8] provided a first-level optimization of CA-based CLM system and proved its utility as a means for separating CO_2 from low-concentration CO_2 sources, such as air and respiratory gas. Given a feed concentration of 0.1% (v/v) CO_2, the selectivity of CO_2/N_2 was 1090, CO_2/O_2 was 790, and CO_2 permeance was 4.71×10^{-8} mol/(m^2 s Pa). The CLM design results in a system that was very stable even in the presence of dry feed and sweep gas. However, the short catalytic lifetime of free enzyme limits their usefulness, and the loss of enzyme solution could not be completely solved.

To improve catalytic stability of enzymes, Cheng et al.[16] reported a hollow fiber contained hydrogel-CA membrane contactor for CO_2 removal from the enclosed spaces. A poly(acrylic acid-*co*-acrylamide) hydrogel was prepared for the immobilization of CA. Activity of immobilized CA could be maintained without apparent reduction during the investigation period of 6 months. By combination of both advantages of CO_2-facilitated transport using CA and the hydrogel, the hydrogel-CA CLM showed good CO_2 removal capability, reducing CO_2 from 0.52% in the inlet feed gas to below 0.090%. These hydrogels have good water retention capacity, and the loss of membrane liquid could be mitigated. However, to compress the volume of the CA-based CLM, CO_2 removal capability should be further improved. This problem could be solved by improving salt absorbency

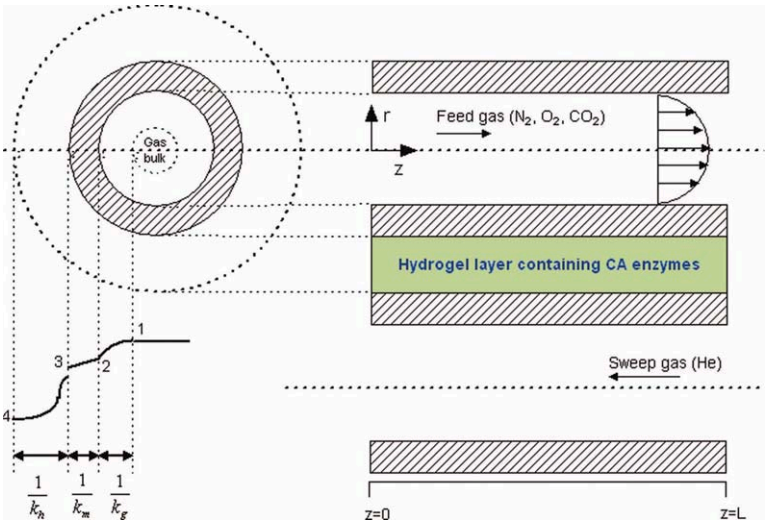

Figure 2. Flow configuration and mass-transfer resistance profiles.

[Color figure can be viewed in the online issue, which is available at wileyonlinelibrary.com.]

of hydrogels. Hydrogels with high salt absorbency could immobilize more CA solution to enhance the performance of the CA-based CLM. Therefore, we have prepared a novel poly(acrylic acid-*co*-acrylamide)/hydrotalcite (PAA-AAm/HT) nanocomposite hydrogel for the CA immobilization.[17,18] Water and salt absorbency of the nanocomposite hydrogel was improved greatly in comparison with common hydrogels. Moreover, immobilized CA maintains the majority of enzymatic activity because of the formation of a microenvironment almost all composed of free water inside the porous network structures of the nanocomposite hydrogel. We have reported the results of developing a novel hollow fiber membrane reactor contained immobilized enzyme for selective separation of low-concentration CO_2 from mixed gas streams.[19] In the reactor, two bundles of PVDF hollow fiber membrane were aligned staggered parallel in a tube module, and PAA-AAm/HT nanocomposite hydrogel was filled between fibers, in which CA enzymes were immobilized. Immobilized CA could retain the majority of enzymatic activity, and thermal stability was also improved. The data showed that this enzyme-based membrane reactor could effectively separate CO_2 at low concentration from mixed gas streams. Prolonged runs lasting 30 h showed that separation performances of the membrane reactor were quite stable.

The immobilized CA-based, hollow fiber membrane reactor to capture CO_2 is a complicated process with large numbers of interdependent variables. Therefore, it is impossible to optimize this system by means of experimental methods alone. Systems analysis and modeling is an important guiding approach. Modeling study on CO_2 separation by facilitated transport membranes immobilized with amine solutions and CA has been reported.[20–23] Differently, in this study, a nanocomposite hydrogel was used to immobilize CA enzyme. It is well known that it is very difficult to obtain the diffusion coefficient of CO_2 in the hydrogel. To simplify the issue, the CO_2 resistance in the hydrogel is proposed according to the experimental results.

In this article, one objective is to obtain CO_2 concentration profiles in the feed gas phase and the membrane wall by numeric simulation. The other objective is to evaluate the performance of the membrane reactor for the separation of low-concentration CO_2 from a CO_2/air mixture by means of both experimental and numerical methods.

Theory

The consecutive transfer processes of CO_2 occur in the hollow fiber membrane reactor filled with immobilized CA enzyme as shown in Figures 1 and 2:

- CO_2 diffuses from the bulk of feed toward the inner surface of feed fiber membrane wall.
- CO_2 diffuses through the feed fiber.
- CO_2 is hydrated to bicarbonate by CA enzyme on the outside surface of feed fiber membrane, and bicarbonate diffuses across the hydrogel layer to the outer surface of sweep fiber membrane.
- Bicarbonate is dehydrated to CO_2 by CA enzyme on the outer surface of sweep fiber, and CO_2 diffuses through sweep fiber.

The diffusion coefficient of CO_2 in the membrane (D_m), which is related with the flow state of CO_2 within the membrane pore, can be determined by Knudsen number (K_n), which is defined as

Table 1. Physicochemical Parameters Used in This Study

Parameter	Values	Source
Mean free path of CO_2 (λ)	39.7 nm	Hirschfelder et al.[24]
Mean free path of O_2 (λ)	54.7 nm	
Mean free path of N_2 (λ)	60 nm	
Knudsen number (K_n)	0.13	Eq. 1
Diffusion coefficient of CO_2 in air (D_g)	1.39×10^{-5} m^2/s	Pritchard and Currie[25]
Knudsen diffusion (D_k)	1.2×10^{-6} m^2/s	Eq. 3
Diffusion coefficient of CO_2 in the membrane (D_m)	4.42×10^{-7} m^2/s	Eq. 2
k_{cat} of CO_2 hydration	7.9×10^5 s^{-1}	Baird et al.[26]
Molecular weight of carbonic anhydrase	30 kDa	Manufacturer

$$K_n = \frac{\lambda}{d_p} \tag{1}$$

In this study, Knudsen number (K_n) is 0.13, and both Knudsen and surface flow diffusions are taken into consideration. The resistance to mass transfer within the membrane is mainly due to the membrane's structure and the presence of a stagnant film within the pore. Therefore, the diffusion coefficient of CO_2 in the membrane (D_m) can be described by Fick's law and defined as

$$D_m = \frac{\varepsilon}{\tau}\left(\frac{1}{D_g} + \frac{1}{D_k}\right)^{-1} \tag{2}$$

Obviously, the diffusion coefficient of CO_2 in the membrane (D_m) is a combination of the diffusion coefficient of CO_2 in air (D_g) and the Knudsen diffusion (D_k), which takes into account the molecules interactions within the pore's wall. In addition, the physicochemical parameters used in this study are shown in Table 1.

The Knudsen diffusion is expressed as[27,28]

$$D_k = \frac{d_p}{3}\sqrt{\frac{8RT}{\pi M_{CO_2}}} \tag{3}$$

The resistance to mass transfer within the hydrogel layer is very complex. In our previous work,[19] the effect of CO_2 concentration and CA concentration on the resistance to mass transfer has been studied in detail. The results showed that CA enzyme could improve the facilitated transport of CO_2 and reduce the transport resistance. On the other hand, higher CO_2 concentration could increase the mass-transfer resistance, and the separation performance of the membrane reactor also decreased. Therefore, the resistance to mass transfer within the hydrogel layer, which is mainly due to the CA enzyme concentration (C_E) and the CO_2 concentration of feed inlet (C_0), can be defined as

$$\frac{1}{k_h} = a\left(\frac{C_0}{C_E}\right)^b \tag{4}$$

Based on the above, assuming the system operated at steady state, the overall mass transfer coefficient (K_{OV}) within the membrane wall and the hydrogel layer can be described as (negligible wall thickness of membranes)

$$\frac{1}{K_{OV}} = \frac{\delta}{D_m} + a\left(\frac{C_0}{C_E}\right)^b = \frac{\delta\tau}{\varepsilon}\left(\frac{1}{D_g} + \frac{1}{D_k}\right) + a\left(\frac{C_0}{C_E}\right)^b \tag{5}$$

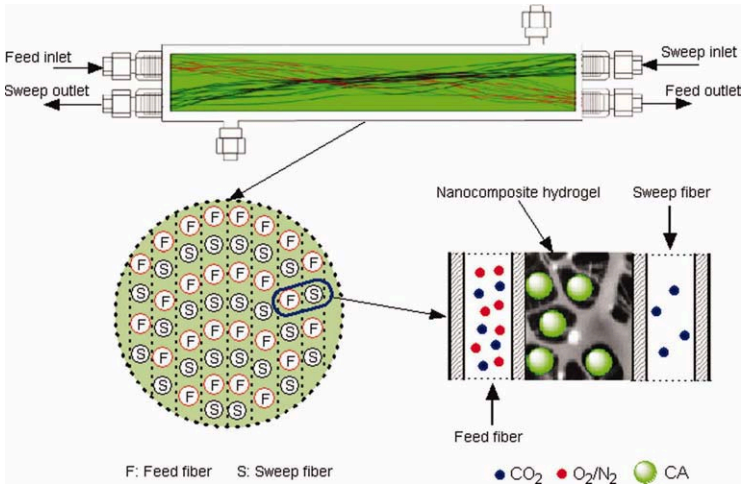

Figure 3. Schematic illustration of hollow fiber contained immobilized enzyme membrane reactor.

[Color figure can be viewed in the online issue, which is available at wileyonlinelibrary.com.]

Mathematical Model

The mathematical model is set based on the following assumptions:

- isothermal conditions and ideal gas behavior;
- steady-state operated system;
- fully developed laminar flow in the feed fiber;
- negligible axial diffusion;
- constant gas pressures; and
- uniform distribution of CA enzyme in the hydrogel layer.

Using these assumptions, the mass-transfer continuous equation in cylindrical coordinates for CO_2 is as shown in Eq. 6

$$v_0 \frac{\partial C}{\partial z} = D_g \frac{1}{r} \frac{\partial}{\partial r}\left(r \frac{\partial C}{\partial r}\right) \tag{6}$$

The above equation is subjected to the following initial and boundary condition

$$\text{at } z = 0, \quad C = C_0; \tag{7}$$

$$\text{at } r = R, \quad -D_g \frac{\partial C}{\partial r} = K_{OV}(C - C_4) \tag{8}$$

As Eq. 6 is second-order partial differential equation, which should be changed to ordinary differential equations by means of variable separation method. If we let $c(r, z) = E(z)\, F(r)$, after the separation of variable method, the ordinary differential equation could be obtained, namely

$$E = A \exp\left(-\frac{D_g}{v_0} \lambda^2 z\right) \tag{9}$$

$$\begin{cases} \frac{d}{dr}\left(r \frac{dF}{dr}\right) + \lambda^2 r F = 0 \\ -D_g \frac{\partial F}{\partial r} = K_{OV} F \end{cases} \tag{10}$$

According to Eq. 10, the following equation (Eq. 11) could be obtained

$$F = AJ_0(\lambda r) + BY_0(\lambda r) \tag{11}$$

For $Y_0(\lambda r)$, owing to the singularity at $r = 0$, then $B = 0$. Therefore, Eq. 11 is transformed to

$$F = AJ_0(\lambda r) \tag{12}$$

In addition, according to the boundary condition, Eq. 13 is obtained

$$D\lambda J_1(\lambda R) = K_{OV} J_0(\lambda R) \tag{13}$$

According to Eq. 13, the eigenvalue, λ_n, could be determined, and the eigenfunction is

$$F_n = J_0(\lambda_n r) \tag{14}$$

Therefore, the solution is

$$c(z, r) = \sum_{n=1}^{\infty} A_n \exp\left(-\lambda_n^2 \frac{D}{v_0} z\right) J_0(\lambda_n r) \tag{15}$$

The coefficient A_n could be determined by initial value, and the result is as follows

$$A_n = \frac{2C_0}{RJ_1(\lambda_n R)\left[1 + \frac{D^2}{K_{OV}^2}\lambda_n^2\right]\lambda_n} \tag{16}$$

Experimental Section

The hollow fiber membrane reactor used in this study is shown in Figure 3, which is constructed by two

Table 2. Specifications of the Membrane Reactor Used in This Study

Characteristics	Values
Fibers material	PVDF
Module length (mm)	580
Module outer diameter (mm)	30
Module inner diameter (mm)	27
Fiber outer diameter (μm)	1200
Fiber inner diameter (μm)	850
Wall thickness of fibers, δ (μm)	175
Number of fibers	53
Fiber length (mm)	500
Fiber porosity ε	0.6
Tortuosity factor τ	1.5
Mean pore diameter, d_p (nm)	300
Total membrane area (m^2)	0.2

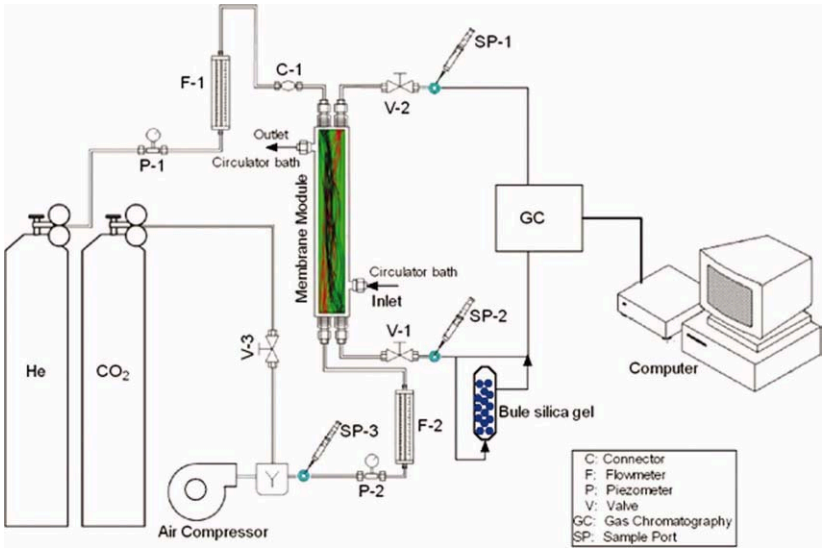

Figure 4. Schematic diagram of experimental setup.

[Color figure can be viewed in the online issue, which is available at wileyonlinelibrary.com.]

independent sets of intimately commingled hydrophobic microporous PVDF hollow fibers prepared by the spinning machine in our laboratory containing immobilized enzyme with nanocomposite hydrogels,[17,18] whose geometrical properties are shown in Table 2. Two nylon meshes were used as the spacer to control the thickness of hydrogel layer, which was about 1.5 mm. The fabrication of the membrane module involved preparation of a fiber bundle and putting them in a shell and finally potting the ends with a resin mixture to form a tube sheet. Two sets of fibers of known length and numbers were placed close to each other, rolled together in the middle up to a particular length while the two ends were kept separate. One set of fibers (27 fibers) carried the feed gas, and the other (26 fibers) carried the sweep gas.

The build experimental setup is shown in Figure 4. The feed gas stream consists of a mixture of CO_2 and air. The desired CO_2 concentration was obtained by an air compressor (Hangzhou Hang Kong Compressor). Delivery of all gases was regulated by mass flow controllers. The feed side pressure was controlled at 5×10^5 Pa by a back-pressure regulator (Tescom, USA). Helium (He) was supplied to the permeate side as a sweep gas, and the pressure was kept constant at almost atmospheric pressure. Compositions of all gas streams were analyzed by a gas chromatograph (GC) (Agilent Model 1790, Agilent Technologies) with TCD detector, which was connected to a chromatograph workstation (Zhida N2000, Zhejiang University, China).

Results and Discussion

Diffusion resistance within the hydrogel layer

The diffusion resistance within the hydrogel layer is very complex, which is mainly due to CO_2 concentration and CA concentration. Therefore, the effect of CO_2 concentration and CA concentration on the diffusion resistance within the hydrogel layer was studied in detail. As is well known, permeance (Q) could be calculated from flux (J) and the partial pressure difference across the membrane (Δp), $Q = J/\Delta p$. The diffusion resistance equals to the reciprocal of

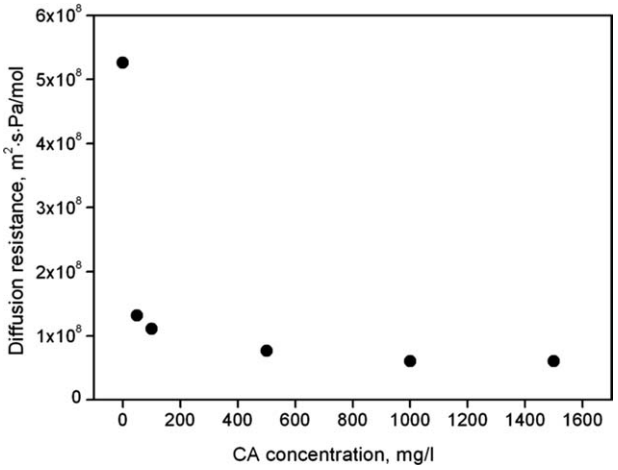

Figure 5. Effect of CA concentration on the diffusion resistance within the hydrogel layer (CO_2 concentration: 0.1%).

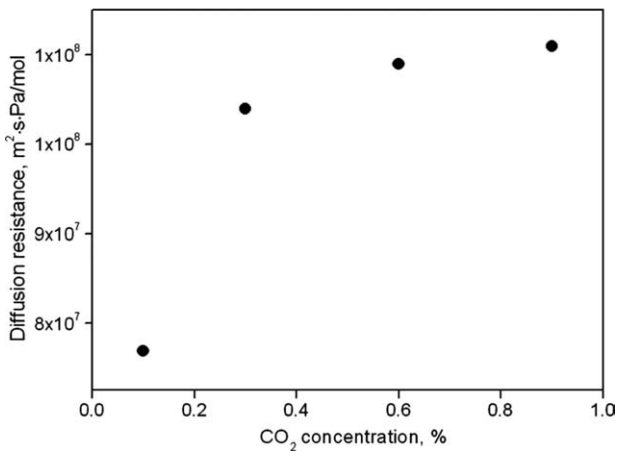

Figure 6. Effect of CO_2 concentration on the diffusion resistance within the hydrogel layer (CA concentration: 1000 mg/L).

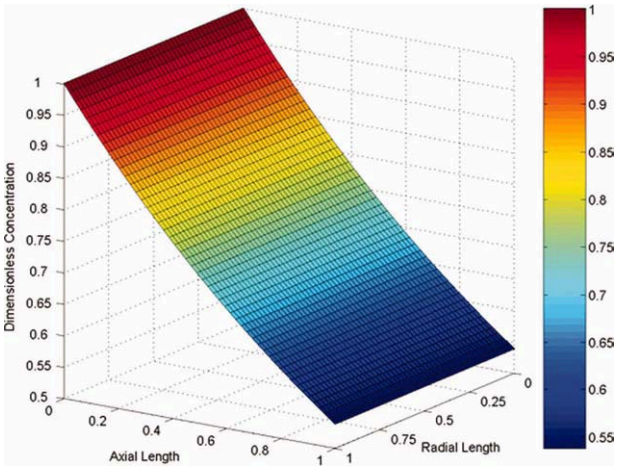

Figure 7. Dimensionless CO_2 concentration in the feed gas phase and the membrane wall at the various radial and axial positions (CO_2 concentration: 0.3%; CA concentration: 1000 mg/L).

[Color figure can be viewed in the online issue, which is available at wileyonlinelibrary.com.]

permeance (Q), $J = \Delta p/(1/Q)$. $1/Q$ is the reciprocal of permeance, which was used as the parameter to evaluate the diffusion resistance. Figure 5 shows the effect of CA concentration on the diffusion resistance within the hydrogel layer. It clearly showed that CA successfully decreases CO_2 diffusion resistance within the hydrogel layer. This is because that the turnover of CA is greater than 1×10^6 s^{-1} making it the fastest known catalyst for the CO_2 hydration reaction, and the actual reaction rate of CO_2 is also proportional to the CA concentration in the hydrogel layer. In addition, from Figure 5, CA concentration is inversely proportional to diffusion resistance, which is nearly a power function model. Figure 6 shows the effect of CO_2 concentration on the diffusion resistance within the hydrogel layer. On the contrary, more CO_2 could increase CO_2 diffusion resistance within the hydrogel layer, and CO_2 concentration is proportional to diffusion resistance, which is also nearly a power function model. This indicates that at the beginning CO_2 was hydrated and dissolved in the hydrogel layer, once bicarbonate ions in the hydrogel layer reached the saturated state, no more CO_2 could be accepted in the hydrogel layer. Thus, CO_2 accumulates on the permeate side and the driving force will decrease gradually and diffusion resistance will increase accordingly. Once the diffusion resistance is large enough, no CO_2 could pass through the membrane resulting in no further separation.

Based on the above, the diffusion resistance within the hydrogel layer, which is mainly due to the CA enzyme concentration (C_E) and the CO_2 concentration of feed inlet (C_0), could be defined as Eq. 4.

CO_2 concentration profiles in the feed gas phase and the membrane wall

From the equations, CO_2 concentration profiles in the feed gas phase and the membrane wall obtained by means of Matlab software are shown in Figure 7. Herein, to show CO_2 removal efficiency more clearly, the dimensionless concentration defined as C/C_0 was used in Figure 7. From the axial view, CO_2 concentration decreases with the increase of Z axis. This is because CO_2 diffusion in the radial direction occurs while axial convection takes place. Then, part of CO_2 diffuses across the enzyme membrane reactor to the sweep side, so CO_2 concentration in the outlet of the feed side would gradually decrease. In the actual experiment, CO_2 concentration including 0.1, 0.3, 0.6, and 0.9% in the inlet of the feed gas could be reduced to 0.052, 0.16, 0.33, and 0.5%, respectively, in the outlet of the feed gas by means of the membrane reactor. CO_2 removal ratio of the membrane reactor is 48, 46.7, 45, and 44.4%, respectively. From Figure 7, CO_2 removal ratio is 46%, and the model prediction is in good agreement with the experimental results.

However, according to Figure 7, CO_2 concentration in the radial has little change, and the concentration profile is almost a straight line. It is mainly because that CO_2 diffusion in the radial is so fast. Therefore, the two-dimensional CO_2 concentration profiles in the feed gas phase (A) and the

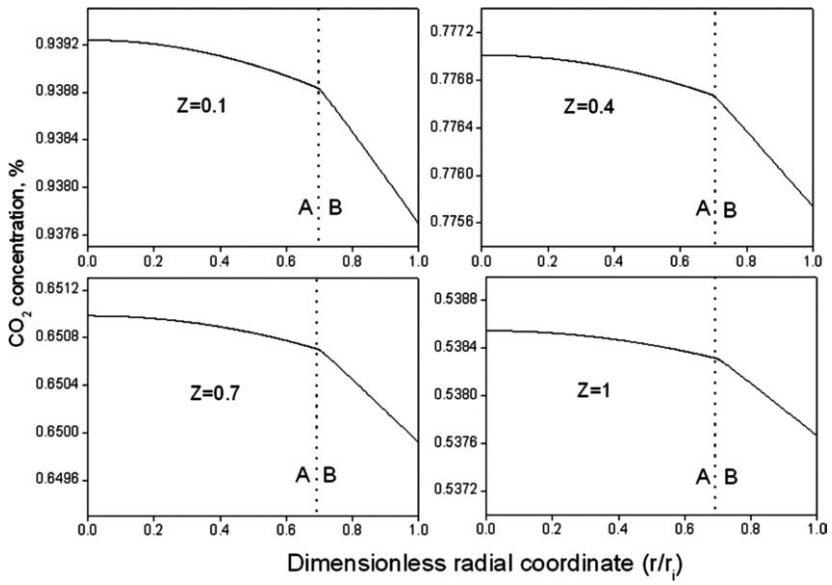

Figure 8. Actual CO_2 concentration in the feed gas phase (A) and the membrane wall (B) at dimensionless radial positions (CO_2 concentration: 0.1%; CA concentration: 1000 mg/L).

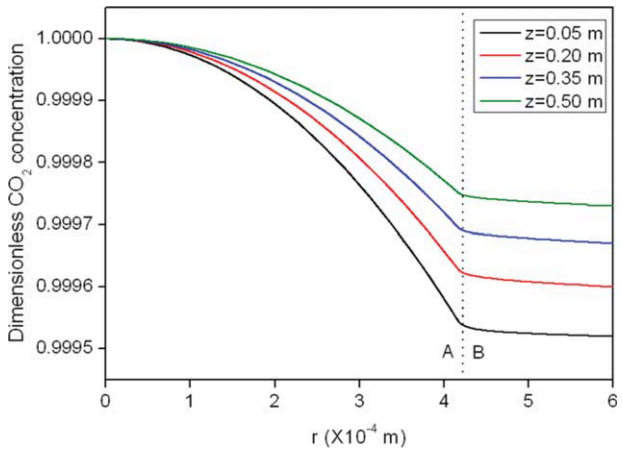

Figure 9. Dimensionless CO_2 concentration in the feed gas phase (A) and the membrane wall (B) at actual radial positions (CO_2 concentration: 0.1%; CA concentration: 1000 mg/L).

[Color figure can be viewed in the online issue, which is available at wileyonlinelibrary.com.]

membrane wall (B) are obtained, as shown in Figures 8 and 9. It is clear that CO_2 concentration in the feed gas phase displays parabola distribution, as shown in Figures 8A and 9A. As the Reynolds number of CO_2 in the feed gas phase is less than 2300, which belongs to the laminar flow. In addition, the parabola trend changes slightly with the increase of Z axis. In the membrane wall, CO_2 molecule diffuses quickly and is approximately Fick diffusion, as shown in Figures 8B and 9B. Moreover, CO_2 concentration and flux distribution in the membrane wall of the feed fiber are also obtained and are shown in Figure 10. Similarly, CO_2 concentration and flux decrease with the increase of Z axis owing to CO_2 diffusion in the radial.

Effect of CO_2 concentration, CA concentration, and flow rate of the feed gas on CO_2 removal performance of the membrane reactor

Figure 11 compares the measured and simulated CO_2 removal performance of the membrane reactor under the various CO_2 concentrations. Obviously, CO_2 removal performance of the membrane reactor decreases as CO_2 concentration in the feed side is increased. CO_2 concentration is a very important impact factor, and separation performance of the membrane reactor is directly influenced by the feed stream CO_2 concentration (pCO_2). Therefore, it is important to investigate the effect of different CO_2 concentrations on the separation performance of the membrane reactor. There is reactive boundary layer in the interface between membrane and hydrogel layer. More CO_2 will gather in the boundary layer with the increase in CO_2 concentration. The boundary layer resistance will increase accordingly. Therefore, the performance of the reactor will decrease. The simulation results are in very good agreement with the measured values at lower feed CO_2 partial pressure with a maximum deviation of up to 14.2%.

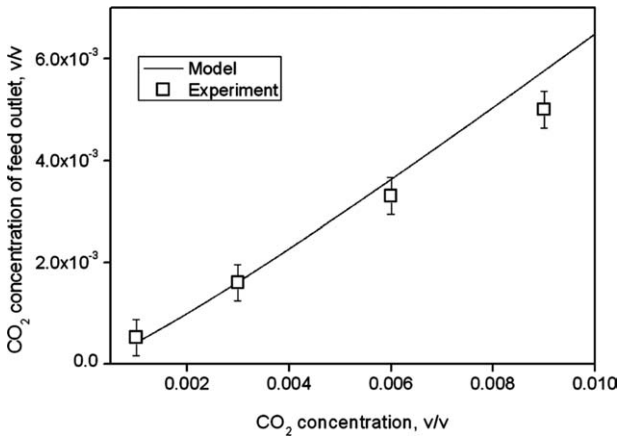

Figure 11. A comparison of the measured and simulated CO_2 removal performance of the membrane reactor under the various CO_2 concentrations (CA concentration: 1000 mg/L).

Figure 12 compares measured and simulated CO_2 removal performance of the membrane reactor under the various CA concentrations. When CO_2 concentration in the feed gas is higher, there would be a demand for greater rates of hydration and dehydration of CO_2 with CA enzyme. Higher CA concentration is required to achieve maximum CO_2 removal capability. When there is no immobilized CA enzyme in the hydrogels, the membrane reactor loses its separation

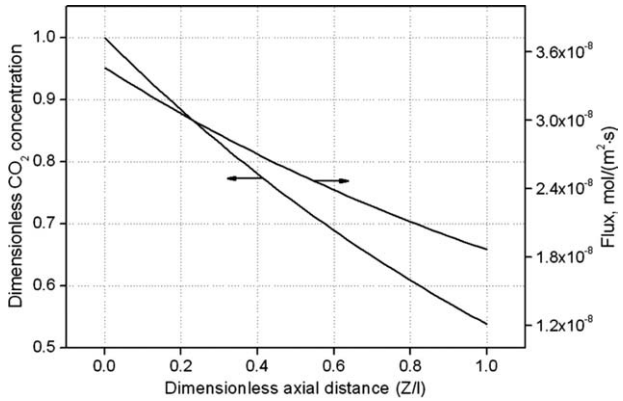

Figure 10. CO_2 concentration and flux distribution in the membrane wall of the feed fiber at the various dimensionless axial distances (CO_2 concentration: 0.1%; CA concentration: 1000 mg/L).

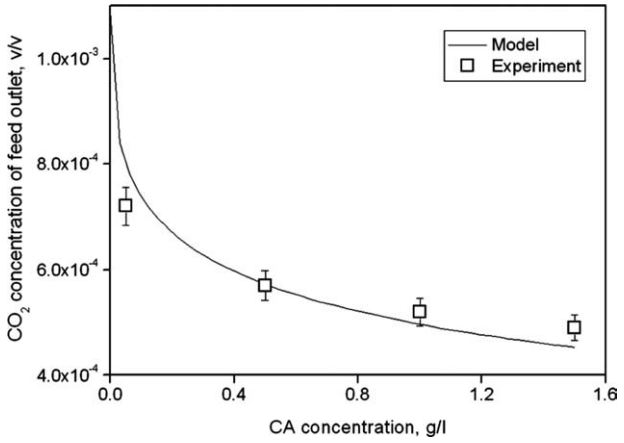

Figure 12. A comparison of the measured and simulated CO_2 removal performance of the membrane reactor under the various CA concentrations (CO_2 concentration: 0.1%).

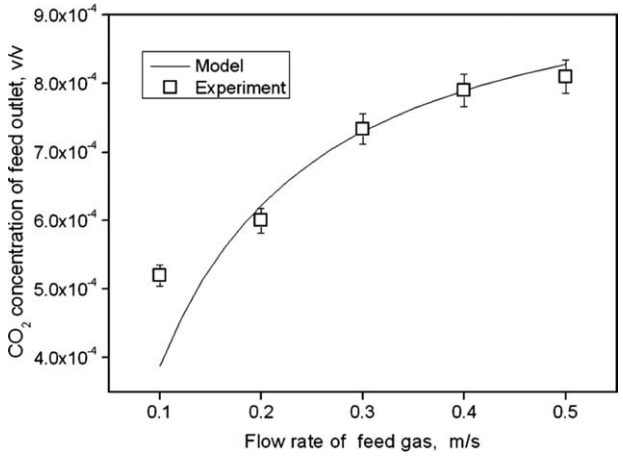

Figure 13. A comparison of the measured and simulated CO_2 removal performance of the membrane reactor under the various flow rates of the feed gas (CO_2 concentration: 0.1%; CA concentration: 1000 mg/L).

performance. It is because that hydrogel layer accounts for the major transport resistance. With addition of CA, the transport resistance decreases markedly. As the solubility of bicarbonate is much more than that of CO_2 in water, the transport capacity for CO_2 is much higher in bicarbonate form than for $CO_{2(aq)}$ even though the diffusivity for $CO_{2(aq)}$ is greater than that for bicarbonate. Bicarbonate transport greatly improved the total CO_2 mass transfer. Therefore, when the CA concentration was low, there was less CA enzyme to hydrate and dehydrate all the CO_2 at a maximum rate. Thus, CO_2 permeance increased with increasing the amount of CA enzyme. Because O_2 and N_2 cannot react with CA enzyme, the selectivity increased as the CA concentration increased. Moreover, the model solution agrees with the experimental data with a maximum deviation of up to 10.2%.

Figure 13 compares measured and simulated CO_2 removal performance of the membrane reactor under the various flow rate of the feed gas. Gas separation usually uses an inert gas such as argon or helium as the sweep gas to remove permeates from the sweep side. To achieve high efficiency

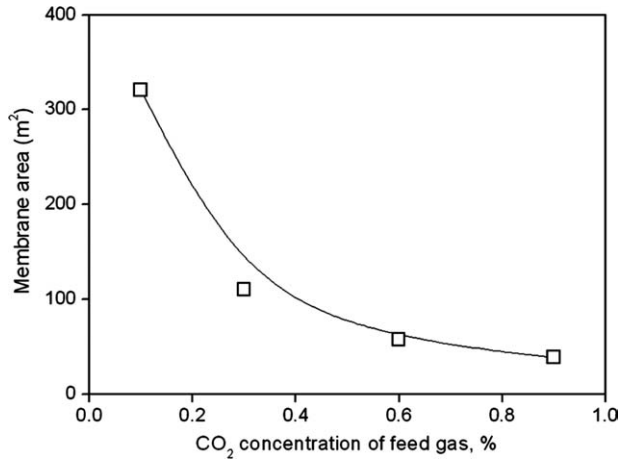

Figure 14. Effect of CO_2 concentration in the feed gas on membrane area requirement for the same CO_2 removal task (1 kg/day) (CA concentration: 1000 mg/L).

Table 3. Comparison of Ideal and Actual CO_2 Turnover Number (CA Concentration: 1000 mg/L)

CO_2 Concentration of Feed Inlet (%)	CO_2 Concentration of Feed Outlet (%)	Ideal CO_2 Turnover Number (mol/s)	Actual CO_2 Turnover Number (mol/s)
0.1	0.052	5.27	1.68×10^{-7}
0.3	0.16	5.27	4.79×10^{-7}
0.6	0.33	5.27	9.24×10^{-7}
0.9	0.5	5.27	13.7×10^{-7}

for the membrane reactor, it is pivotal to control the flow rate of feed and sweep gas. The appropriate flow rate of feed and sweep gases could enhance the specific surface area of the gas–liquid contact to improve the removal efficiency. We found that CO_2 transport could be facilitated if the flow rate in the feed side was lower than that in the sweep side. As the flow rate of the feed gas increased, CO_2 could accumulate on the permeate side and the driving force would decrease gradually. Once the driving force was small enough, CO_2 could not pass through the membrane and hydrogel layer efficiently. If higher flow rate of the feed gas was used, CO_2 on the permeate side could not be moved efficiently. On the other hand, the boundary layer thickness of the gas phase in the sweep side decreases with the increasing flow rate in the sweep side, which has an effect of decreasing the mass-transfer resistance resulting in a slight increase in the mass diffusion.[27] Consequently, a moderate flow rate of the feed gas and sweep gas is good selection to produce high driving force. The numerically calculated results are in reasonable agreement with the experimentally generated data with a maximum deviation of up to 18.7%.

These deviations between model solution and experimental data are mainly due to the determination of the membrane and hydrogel layer resistance. In addition, Boucif et al.[27] have proposed that the essential reason to this difference is probably that the membrane assumed to be completely dry was partially wetted as a result of the gas and liquid fluctuating pressures. In this study, the hollow fiber membranes were partially wetted as a result of the gas and hydrogel layer fluctuating pressures.

Membrane area requirement for the same CO_2 removal task

The effect of CO_2 concentration in the feed gas on membrane area requirement for the same CO_2 removal task (1 kg/day) was obtained and shown in Figure 14. CO_2 removal technologies in life-support systems must be safe and reliable, which is characterized by small volume, low mass, low rate of energy use, minimal use of consumables, and simple and convenient operation. Therefore, the required membrane area for the same CO_2 removal task should be as little as possible. The results showed that higher CO_2 concentration in the feed gas can significantly reduce the required membrane area. In addition, we compared the actual and ideal utilization rate of CA enzyme in the membrane reactor, and the results are shown in Table 3. Obviously, the actual and ideal utilization rate of CA enzyme is very low. It is because that enzyme distribution in the hydrogel layers of the membrane reactor might also limit the role of CA enzyme for the hydration and dehydration reaction. This could cause that CA enzyme could not be all involved in the catalyzed reaction. Therefore, if the actual utilization rate of CA

enzyme is improved further, the required membrane area for the same CO_2 removal task would be lower.

Conclusion

CO_2-facilitated transport across a hollow fiber membrane reactor filled with immobilized CA by nanocomposite hydrogel was evaluated through experiment and simulation. CO_2 concentration profiles in the feed gas phase and the membrane wall were achieved by numeric simulation. The effects of CO_2 concentration in the feed gas, CA concentration, and flow rate of feed gas on CO_2 removal performance were also investigated in detail, and our predictions are in very good agreement with the measured values. Moreover, the effect of CO_2 concentration on the required membrane areas for the same CO_2 removal target (1 kg/day) was studied. Higher CO_2 concentration in the feed gas can significantly reduce the required membrane area. If the actual utilization rate of CA enzyme is improved further, the required membrane area for the same CO_2 removal task would be lower.

Acknowledgments

The authors gratefully acknowledge support from the National Natural Science Foundation of China (No. 20776123), the National High Technology Research and Development Program of China (2008AA06Z330), Science Foundation of Chinese University, and Innovation Scientists and Technicians Troop Construction Projects of Zhengzhou City.

Notation

C_0 = CO_2 concentration in the feed inlet, v/v
C_E = CA enzyme concentration, mg/L
D_g = diffusion coefficient of CO_2 in air, m^2/s
D_k = Knudsen diffusion coefficient, m^2/s
D_m = diffusion coefficient of CO_2 in the membrane, m^2/s
d_p = mean pore diameter, nm
K_n = Knudsen number
K_{OV} = overall mass transfer coefficient, m/s
v_0 = flow rate of the feed gas, m/s

Greek letters

λ = mean free path, nm
τ = membrane's pore tortuosity
δ = wall thickness of fibers, μm
ε = membrane's porosity

Literature Cited

1. Ackerman KV, Sundquist ET. Comparison of two U.S. power-plant carbon dioxide emissions data sets. *Environ Sci Technol*. 2008;42:5688–5693.
2. Supra LN, Brasseux S. Molecular sieve CO_2 removal systems: international space station and Lunar-Mars life support test project. *SAE Trans*. 1997; 972419.
3. Filburn TP, Nalette TA, Graf JC. The design and testing of a fully redundant regenerative CO_2 removal system (Rcrs) for the shuttle orbiter. *SAE Trans*. 2001;2001-01-2420.
4. Adachi T, Miya A. Microalgae culturing reactor for carbon dioxide elimination and oxygen recovery-CO_2 fixation activity under various irradiation cycle. *SAE Trans*. 1994; 941412.
5. Bolsunover A, Zhavoronks V. Prospects for using microalgae in life-support system. *SAE Trans*. 1995; 951496.
6. Fan LH, Zhang YT, Zhang L, Chen HL. Evaluation of a membrane-sparged helical tubular photobioreactor for carbon dioxide biofixation by *Chlorella vulgaris*. *J Membr Sci*. 2008;325:336–345.
7. Zhang YT, Fan LH, Zhang L, Chen HL. Research progress in removal of trace carbon dioxide from closed spaces. *Front Chem Eng China*. 2007;1:310–316.
8. Cowan RM, Ge JJ, Qin YJ, McGregor ML, Trachtenberg MC. CO_2 capture by means of an enzyme-based reactor. *Ann N Y Acad Sci*. 2003;984:453–469.
9. Pocker Y, Bjorkquist DW. Stopped-flow studies of carbon dioxide hydration and bicarbonate dehydration in water and water-d2. Acid-base and metal ion catalysis. *J Am Chem Soc*. 1977;99:6537–6543.
10. Duda D, Tu C, Qian M, Laipis P, Agbandje-McKenna M, Silverman DN, McKenna R. Structural and kinetic analysis of the chemical rescue of the proton transfer function of carbonic anhydrase II. *Biochemistry*. 2001;40:1741–1748.
11. Elder I, Han S, Tu C, Steele H, Laipis PJ, Violar RE, Silverman DN. Activation of carbonic anhydrase II by active-site incorporation of histidine analogs. *Arch Biochem Biophys*. 2004;421:283–289.
12. Enns T. Facilitation by carbonic anhydrase of carbon dioxide transport. *Science*. 1967;155:44–47.
13. Suchdeo SR, Schultz JS. Mass transfer of CO_2 across membranes: facilitation in the presence of bicarbonate ion and the enzyme carbonic anhydrase. *Biochim Biophys Acta*. 1974;352:412–440.
14. Kemperman AJB, Bargeman D, Boomgaard TVD, Strathmann H. Stability of supported liquid membrane: state of the art. *Sep Sci Technol*. 1996;31:2733–2762.
15. Guha AK, Majumdar S, Sirkar KK. Gas separation modes in a hollow fiber contained liquid membrane permeator. *Ind Eng Chem Res*. 1992;31:593–604.
16. Cheng LH, Zhang L, Chen HL, Gao CJ. Hollow fiber contained hydrogel-CA membrane contactor for carbon dioxide removal from the enclosed spaces. *J Membr Sci*. 2008;324:33–43.
17. Zhang YT, Fan LH, Zhi TT, Zhang L, Huang H, Chen HL. Synthesis and characterization of poly (acrylic acid-co-acrylamide)/hydrotalcite nanocomposite hydrogels for carbonic anhydrase immobilization. *J Polym Sci Part A: Polym Chem*. 2009;47:3232–3240.
18. Zhang YT, Zhi TT, Zhang L, Huang H, Chen HL. Immobilization of carbonic anhydrase by embedding and covalent coupling into nanocomposite hydrogel containing hydrotalcite. *Polymer*. 2009;50:5693–5700.
19. Zhang YT, Zhang L, Chen HL, Zhang HM. Selective separation of low concentration CO_2 using hydrogel immobilized CA enzyme based hollow fiber membrane reactors. *Chem Eng Sci*. 2010;65:3199–3207.
20. Guha AK, Majumdar S, Sirkar KK. Facilitated transport of CO_2 through an immobilized liquid membrane of aqueous diethanolamine. *Ind Eng Chem Res*. 1990;29:2093–2100.
21. Gorji AH, Kaghazchi T. CO_2/H_2 separation by facilitated transport membranes immobilized with aqueous single and mixed amine solutions: experimental and modeling study. *J Membr Sci*. 2008;325:40–49.
22. Bao L, Trachtenberg MC. ModelingCO_2-facilitated transport across a diethanolamine liquid membrane. *Chem Eng Sci*. 2005;60:6868–6875.
23. Bao L, Trachtenberg MC. Facilitated transport of CO_2 across a liquid membrane: comparing enzyme, amine, and alkaline. *J Membr Sci*. 2006;280:330–334.
24. Hirschfelder JO, Curtiss CF, Bird RB. *The Molecular Theory of Gases and Liquids*. New York: Wiley, 1964.
25. Pritchard DT, Currie JA. Diffusion of coefficients of carbon dioxide, nitrous oxide, ethylene and ethane in air and their measurement. *Eur J Soil Sci*. 2006;33:175–184.
26. Baird TT Jr, Waheed A, Okuyama T, Sly WS, Fierke CA. Catalysis and inhibition of human carbonic anhydrase IV. *Biochemistry*. 1997;36:2669–2678.
27. Boucif E, Favre E, Roizard D, Belloul M. Hollow fiber membrane contactor for hydrogen sulfide odor control. *AIChE J*. 2008;54:122–131.
28. Boucif E, Favre E, Roizard D. CO_2 capture in HFMM contactor with typical amine solutions: a numerical analysis. *Chem Eng Sci*. 2008;63:5357–5385.

Manuscript received Oct. 9, 2010, and revision received Jun. 20, 2011.